Hydrothermal fluid venting along a seismogenic detachment fault in the Moresby rift (Woodlark basin, Papua New Guinea)

Vincent Famin, Satoru Nakashima

Geochemistry Geophysics Geosystems G3
AN ELECTRONIC JOURNAL OF THE EARTH SCIENCES
Published by AGU and the Geochemical Society

Article
Volume 6, Number 12
22 December 2005
Q12003, doi:10.1029/2005GC001112
ISSN: 1525-2027

Hydrothermal fluid venting along a seismogenic detachment fault in the Moresby rift (Woodlark basin, Papua New Guinea)

Vincent Famin
Laboratoire des Sciences de la Terre, Université de la Réunion, 15 Avenue René Cassin, BP 7151, F-97715 Saint Denis Messag Cedex 9, La Réunion, France (vfamin@univ-reunion.fr)

Satoru Nakashima
Department of Earth and Space Science, Graduate School of Science, Osaka University, 1-1 Machikaneyama-cho, Toyonaka-shi, Osaka 560-0043, Japan

[1] We investigate the conditions of hydrothermal alteration occurring along an active, seismogenic normal fault dipping <30° in the Moresby rift (Woodlark basin, Papua New Guinea). Petrological and fluid inclusion studies were conducted in the samples recovered from the Ocean Drilling Program leg 180 that cored the footwall, scarp, and hanging wall of the fault. Chemical analyses of the thermodependent Si-Al substitutions in chlorites show that synrift alteration is coeval with a temperature rise from 200°C to 300°C in the footwall of the detachment, whereas no thermal event is recorded in the hanging wall. In the same samples, fluid inclusions indicate that footwall rocks followed an isothermal exhumation path from 5–7 km to the subsurface. Taken together, the results strongly suggest that the +100°C temperature rise results from the upward migration of H_2O-NaCl fluids expelled by dehydrating metamorphic rocks from the lower crust. Fluid release began with the onset of detachment faulting and is still actively occurring nowadays. The fact that low-angle earthquakes also occur now at 5–7 km along the fault suggests that the dehydration of the metamorphic rocks and the subsequent circulation of hot hydrothermal fluids may be responsible for the weakening of the middle crust and the formation of a detachment in the Moresby rift.

Components: 9370 words, 7 figures, 1 table.

Keywords: chlorite; detachment fault; fluid inclusions; hydrothermal fluid; Woodlark basin.

Index Terms: 3653 Mineralogy and Petrology: Fluid flow; 8045 Structural Geology: Role of fluids; 8163 Tectonophysics: Rheology and friction of fault zones (8034).

Received 10 August 2005; **Revised** 20 September 2005; **Accepted** 7 November 2005; **Published** 22 December 2005.

Famin, V., and S. Nakashima (2005), Hydrothermal fluid venting along a seismogenic detachment fault in the Moresby rift (Woodlark basin, Papua New Guinea), *Geochem. Geophys. Geosyst.*, *6*, Q12003, doi:10.1029/2005GC001112.

1. Introduction

[2] Detachments are crustal-scale normal faults dipping <30° that progressively expose rocks from deep structural levels in the lower crust. These faults are mechanically intriguing because they are oriented at high angle relative to the regional maximum principal stress σ_1 in rifts, and therefore require an extremely low apparent coefficient of friction of rocks in order to initiate and slip [*Wernicke*, 1981]. A similar low apparent frictional strength also explains the slip of the San Andreas fault despite its misorientation relative to the regional maximum horizontal stress [*Zoback et al.*, 1985].

[3] Some theoretical models have proposed that the low frictional strength of "weak" faults may result from fluid-rock interactions, either by in-

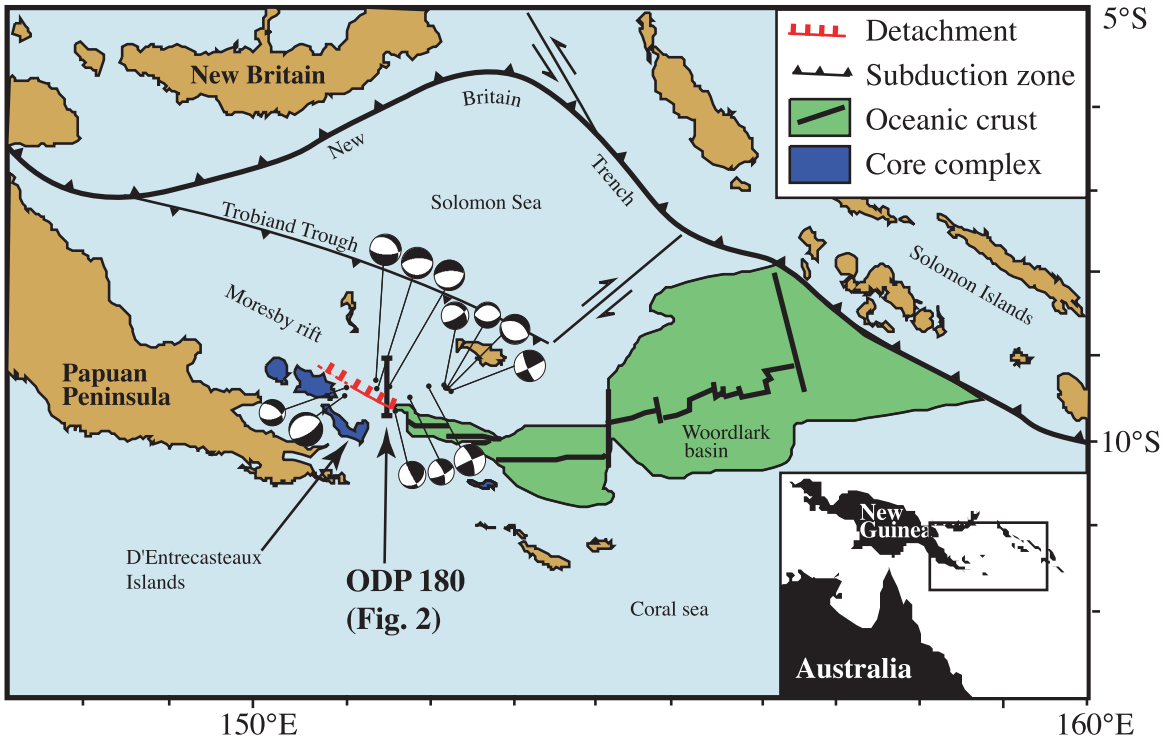

Figure 1. Regional and tectonic map of the Papua New Guinea area, showing the location of the ODP leg 180 campaign (modified from *Shipboard Scientific Party* [1999a]).

creasing the pore pressure [*Sibson*, 1985; *Axen*, 1992; *Rice*, 1992] or by inducing an alteration of hard minerals into weak phyllosilicates [*White and Knipe*, 1978; *Wintsch et al.*, 1995]. Both of these explanations rely on the implicit assumption that fluid supply must predate the initiation of the fault zone, and last the whole lifetime of fault activity in order to explain its low frictional strength. However, the only direct record of these fluid-assisted weakening processes is the hydrothermal alteration displayed by exhumed detachment zones cropping out in the U.S. Basin and Range or in the Aegean sea [*Glazner and Bartley*, 1991; *Axen*, 1992; *Fricke et al.*, 1992; *Wickham and Peters*, 1992; *Morrison*, 1994; *Losh*, 1997; *Famin et al.*, 2004; *Jolivet et al.*, 2004]. These final stage examples provide few constraints on the timing of fluid-rock interactions relative to the onset of low angle faulting, and no consensus has been reached regarding the "chicken and egg" problem of fluid supply in weak fault zones.

[4] The Moresby detachment in the Woodlark basin (Papua New Guinea) represents the only confirmed example of a modern, seismogenic detachment cropping out on the Earth's surface (Figure 1). This detachment is actively unroofing metamorphic core complexes at an extremely fast rate since the Pliocene [*Hill et al.*, 1992]. The fault has also produced shallow-dipping normal earthquakes up to Mw = 6.2 in the past decades [*Abers*, 1991; *Abers et al.*, 1997]. Furthermore, the shallow dip of the fault is confirmed to a depth of 5–6 km by multichannel seismic reflection data [*Floyd et al.*, 2001], and the footwall, scarp and hanging wall of the fault have been cored offshore during the Ocean Drilling Program (ODP) leg 180 [*Taylor and Huchon*, 2002]. These features make the Moresby detachment a unique living opportunity to study the effect of fluids on the initiation and slip of weak faults. In this paper, we combine mineralogical and fluid inclusion studies to determine the pressure and temperature conditions of hydrothermal alteration in the footwall of the fault, together with the composition and source of the fluids. These data are then compared with present-day geophysical data on the active fault, in order to investigate the fluid-deformation relationship leading to the development of the detachment.

2. Tectonic Setting

[5] The Papuan Peninsula originated in the Paleocene as a fragment detached from Australia by the opening of the Coral sea [*Weissel and Watts*, 1979].

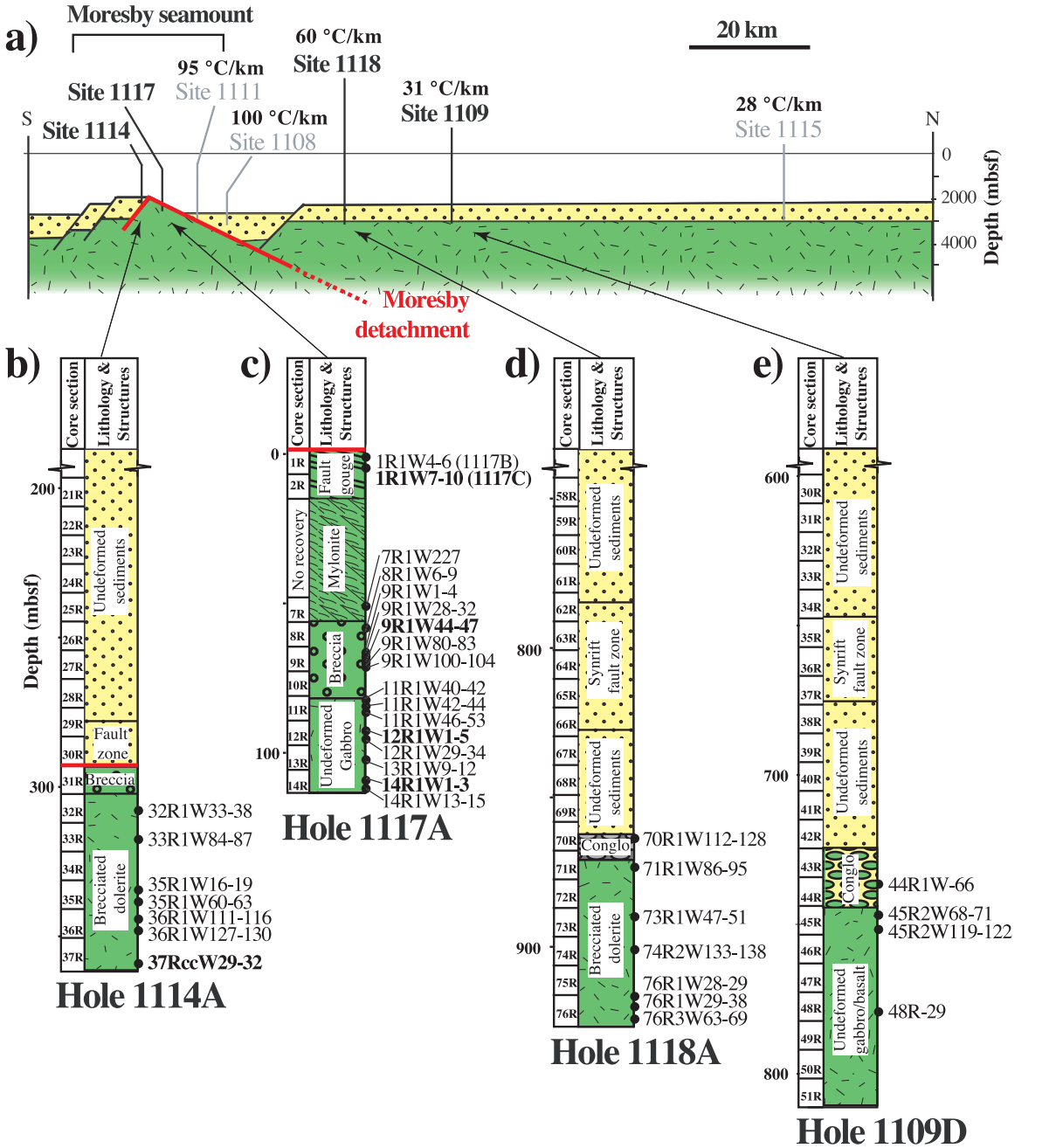

Figure 2. (a) N-S cross section of the Moresby rift, showing the location of the ODP leg 180 drilling sites in the vicinity of the Moresby seamount. (b–e) Lithostratigraphic logs of the four wells that reached the crystalline basement (compiled from *Shipboard Scientific Party* [1999a] and *Gardien et al.* [2002], to which the reader is referred for a complete description of the cores). Also reported is the position of the analyzed samples in the cores. Bold entries correspond to the samples containing fluid inclusions.

As this fragment moved northward it was partially subducted below the Salomon sea. Northward subduction later ceased, ophiolites were obducted onto the Papuan peninsula, and subduction reversed along the Trobiand trough in the Early Miocene [*Davies and Warren*, 1988, and references therein]. Southward subduction led to arc magmatism throughout Miocene to Holocene times.

[6] Seafloor spreading in the easternmost Woodlark basin split the arc 8 Ma ago and propagated

westward [*Karner et al.*, 1993]. Since 5 Ma, seafloor spreading laterally evolved into a continental extension that opened the Moresby rift [*Martinez et al.*, 2001] (Figure 1). Normal slip along the Moresby detachment began with the onset of rifting, as suggested by synrift sediments [*Huchon et al.*, 2002]. Core complexes, now cropping out on the D'Entrecasteaux islands (Figure 1), were exhumed from >10 kbar (35 km) and 570–730°C to the subsurface in about 4 Ma, and are still actively uplifted [*Hill et al.*, 1992; *Baldwin et al.*, 1993]. The rising core complexes breached the cover of obducted ophiolites. Eastward and offshore, the fault is exposed on the northern flank of the Moresby seamount, a crustal block just ahead of the seafloor spreading tip (Figure 2a). The northern flank of the Moresby seamount corresponds to the scarp of the detachment fault, whereas the southern flank was elevated by the slip of a secondary normal fault, antithetic to the main detachment and steeply dipping south (Figure 2a). The geometry of these two antithetic normal faults confirms that at least one of them initiated as a true shallow-dipping detachment, and was not brought to an apparent shallow dip by a domino-style rotation of the crustal blocks [*Huchon et al.*, 2002].

3. Summary of ODP Leg 180 Results

[7] During the ODP leg 180 campaign, a N-S transect of 11 sites (1108 to 1118) was drilled in the Moresby seamount (Figure 2). Four of these sites (1114, 1117, 1118 and 1109) reached the crystalline basement composed of dolerite, gabbro and basalt belonging to the Papuan ophiolite belt (Figures 2b–2e). Sites 1118 and 1109 are located north of the detachment on the hanging wall margin (Figure 2a). Site 1117, located on the crest of Moresby seamount, drilled the footwall scarp of the fault zone itself. Further south in the footwall, site 1114 drilled the secondary high-angle normal fault that flanks the southern side of Moresby seamount. Well-preserved primary magmatic textures have been recovered at all sites [*Gardien et al.*, 2002]. Dolerite from all sites shows an ophitic texture of clinopyroxene, plagioclase and iron oxide or sulphide grains. Basalt found at site 1109 is composed of dark groundmass with quenched structures and microlithes of plagioclase. Gabbro recovered from site 1117 shows a medium-grained texture composed of euhedral laths of plagioclase, subhedral clinopyroxene and xenomorphic quartz grains. These primary magmatic minerals indicate that igneous intrusions occurred at shallow level (0.4 Gpa [*Gardien et al.*, 2002]). Magmatic crystallization was dated 66.4 ± 1.5 Ma by U/Pb on zircons [*Monteleone et al.*, 2002].

[8] In all the mafic rocks, the primary mineralogy is locally replaced by various amounts of undeformed secondary phases (hornblende, plagioclase, chlorite, epidote, zoisite, titanite and zeolite) indicating a static retrograde overprint in the greenschist facies (~200°C, 0.2–0.3 GPa [*Gardien et al.*, 2002]). Ar/Ar dating indicates that this static retrogression occurred 31 ± 0.9 Ma ago [*Monteleone et al.*, 2002]. However, a fraction of these secondary minerals may also have crystallized during the rifting initiated at 5 Ma.

[9] In addition to this anterift stage of static greenschist retrogression, extensional joints filled with hydrothermal assemblages composed of zeolite, quartz, chlorite and calcite are locally found cutting across the undeformed rocks. These joints filled with secondary minerals are clearly associated with the extension of the Moresby rift, and then define a second stage of synrift alteration [*Gardien et al.*, 2002]. Most of the igneous rocks cored on the hanging wall (1118, 1109) display only little evidence of this synrift event (Figures 2d and 2e), whereas cores recovered from footwall sites (1114, 1117) are strongly deformed and altered (Figures 2b and 2c). At site 1117 in the fault scarp, a talc-chlorite-serpentine gouge was recovered in the uppermost 12 meters below seafloor (mbsf). Immediately underneath, a calcite-talc-serpentine mylonite occupies a 50 m thick core section of very low recovery. Calcite-filled veins emplaced parallel to the foliation indicate that shearing occurred under high pore pressure (fluid pressure $P_f \geq$ lithostatic pressure P_l). Further downhole, shearing evolves into a cataclasite of pyroxene, amphibole and epidote fragments embedded in a dark brown matrix composed of zeolite and clays. Chlorite-filled shear planes locally crosscut the cataclasite. Successive generations of quartz-epidote-chlorite veins are observed both cutting across the breccia or crosscut by the breccia. These veins also occur as vertical extensional joints cutting across the fresh gabbro at the bottom of the hole. The whole sequence recovered at site 1117 defines a 100 m thick fault zone in which brittle brecciation and veining is progressively overprinted by ductile shearing toward the fault [*Shipboard Scientific Party*, 1999a]. Mylonites are themselves crosscut by a later stage of veining associated to a final brittle deformation [*Roller et al.*, 2001]. A similar evolution is also described for

the gabbros recovered from hole 1114 in the secondary antithetic normal fault. At both sites, shearing was assisted by fluid-fracturing under high pore pressure. Low carbon, oxygen and boron isotopic ratios in calcite veins suggest that dehydration and decarbonation of high-grade metamorphic rocks is the source of the hydrothermal fluids [*Kopf et al.*, 2003]. Fluid composition evolved from siliceous-rich at the earliest stage of brittle deformation and deeper in the crystalline basement, to carbonate-rich during the later stage of ductile deformation at shallower level [*Shipboard Scientific Party*, 1999b]. Interestingly, borehole geophysical measurements also revealed increasing pore pressures and increasing thermal gradients up to 100°C/km around the main fault [*Kemerer and Screaton*, 2002]. A flow of warm fluids has been detected above the Moresby detachment (site 1108), likely explaining the pore pressure and temperature anomalies [*Shipboard Scientific Party*, 1999a].

4. Analytical Methods

4.1. Chlorite Thermometry

[10] The composition of chlorites was analyzed in 30 μm and 100 μm thick sections cut from core samples recovered at sites 1109, 1118, 1117 and 1114. Analyses were made using a JEOL JXA8800R electron probe micro-analysis (EPMA) at the Tokyo Institute of Technology, with a regulated beam current of 12 nA, an acceleration voltage of 15 keV, and 10 s counting times. Element concentrations were calibrated against a kaersutite amphibole standard using the same procedure for all the analytical sessions. The analytical spot was routinely set at 3–5 μm keeping the same electron beam conditions.

[11] In order to reduce the risk of analyzing mica-chlorite intergrowth instead of pure chlorites, analyses showing more than 1% ($Na_2O + K_2O + CaO$) were rejected. This resulted in the removal of less than 5% of the analyses in Site 1114 samples, 15% in Sites 1117 and 1118 samples, and up to 30% in Site 1109 samples. Since the bulk rock geochemistry is basically the same at all drilling sites, the composition of chlorites is assumed to be essentially temperature dependent. Temperatures were therefore calculated from chlorite compositions using the Cathelineau and Nieva empirical geothermometer based on the Al_{IV} occupancy [*Cathelineau and Nieva*, 1985]. This thermometer has the advantage over more recent ones of dealing with high Si-content chlorites ($2.9 < Si < 3.6$ atom per function unit, or apfu) in the low pressure and low temperature range (0–0.5 GPa; 100–300°C). Structural formulae were calculated on a basis of 14 oxygens (half formula). All iron was assumed to be divalent.

4.2. Microthermometric Analyses

[12] Doubly polished sections extracted from core samples of holes 1117 and 1114 were studied under the microscope in order to characterize the pattern of fluid inclusions. Only inclusions contained in quartz were selected for microthermometry. Microthermometric measurements were performed on Linkam THMSG 600 heating/freezing stage, following procedures outlined by *Roedder* [1984]. The calibration of the stage was made using Synflinc CO_2 and H_2O synthetic fluid inclusion standards at −56.6, 0 and 374°C [*Schmidt and Bodnar*, 2000, and references therein]. The accuracy of measurements was found to be ±0.2°C at low temperature and ±2°C at high temperature. Last melting temperatures were observed at heating rates of 1°C/min after freezing at −90°C. Homogenization temperatures were observed at 1–5°C/min rates, depending on the inclusion size. Bulk thermodynamic properties of fluids were computed from microthermometric data using the MacFlinCor software [*Brown*, 1989]. Salinity (expressed in wt% NaCl equivalent) and density isochores of H_2O-NaCl inclusions were calculated from ice melting and homogenization temperatures using the *Kerrick and Jacobs* [1981] equation of state. The composition and isochores of H_2O-CO_2-CH_4-NaCl inclusions were determined from the volumetric proportions between carbonic and H_2O phases at room temperature, and the temperatures of carbonic phases melting, clathrate melting, CO_2 homogenization and complete homogenization using the *Bowers and Helgeson* [1983] equation of state.

5. Results

5.1. Chlorite Compositions and Temperature Estimates

[13] The composition of chlorites from the Moresby rift is summarized in Table 1. Figure 3 shows the Si-content of chlorites calculated from the ~250 retained EPMA analyses performed on ODP leg 180 samples. Anterift chlorites (crystallized as a static replacement of the primary mineralogy) from all sites (1114, 1117, 1118 and 1119) display a Si-content between 2.95 and 3.45 apfu,

Table 1 (Representative Sample). Summary of Averaged EPMA Analyses on Chlorites From Leg ODP 180 [The full Table 1 is available in the HTML version of this article at http://www.g-cubed.org.]

	Hole 1114A											
Sample	32R1W33-38	33R1W84-87		35R1W16-19		35R1W60-63		36R1W111-16		36R1W127-130	37RccW29-32	
Depth, mbsf	296	306		325		325		335		335	346	
Chlorite texture	Synrift	Anterift	Synrift	Anterift	Synrift	Anterift	Synrift	Anterift	Synrift	Synrift	Anterift	Synrift
No. of analyses	5	1	11	2	8	1	8	4	6	7	1	2
SiO_2	27.15	28.52	26.93	29.02	27.50	27.60	26.84	29.48	27.06	27.08	29.01	27.88
Al_2O_3	18.35	17.15	18.05	17.65	18.36	18.89	17.67	16.37	18.26	17.83	18.43	18.13
FeO	23.50	27.11	27.13	23.64	24.55	26.60	26.58	25.75	26.27	25.73	22.52	20.97
MnO	0.31	0.32	0.34	0.33	0.36	0.29	0.33	0.27	0.34	0.31	0.29	0.23
MgO	16.30	13.77	13.90	16.83	15.90	14.14	13.94	15.01	13.87	13.99	16.25	18.66
CaO	0.18	0.34	0.09	0.54	0.21	0.09	0.15	0.25	0.13	0.36	0.47	0.00
Na_2O	0.13	0.02	0.02	0.02	0.03	0.00	0.04	0.05	0.03	0.09	0.03	0.01
K_2O	0.01	0.00	0.01	0.01	0.01	0.00	0.03	0.05	0.02	0.03	0.00	0.00
Cr_2O_3	0.02	0.06	0.01	0.03	0.01	0.04	0.01	0.02	0.01	0.06	0.01	0.01
TiO_2	0.02	0.03	0.01	0.01	0.03	0.02	0.01	0.01	0.01	0.31	0.06	0.01
Total, wt%	86.18	87.32	86.50	88.08	86.95	87.68	85.60	87.25	85.99	85.80	87.07	85.90
Si	2.89	3.04	2.91	3.01	2.91	2.92	2.92	3.12	2.92	2.93	3.02	2.93
Al	2.30	2.15	2.30	2.16	2.29	2.36	2.27	2.04	2.33	2.27	2.26	2.24
Fe	2.09	2.42	2.45	2.05	2.17	2.35	2.42	2.28	2.38	2.33	1.96	1.84
Mn	0.03	0.03	0.03	0.03	0.03	0.03	0.03	0.02	0.03	0.03	0.03	0.02
Mg	2.58	2.19	2.24	2.60	2.51	2.23	2.26	2.37	2.23	2.25	2.52	2.92
Ca	0.02	0.04	0.01	0.06	0.02	0.01	0.02	0.03	0.01	0.04	0.05	0
Na	0.03	0	0	0	0.01	0	0.01	0.01	0.01	0.02	0.01	0
K	0	0	0	0	0	0	0	0.01	0	0	0	0
Total (apfu)	9.99	9.88	9.95	9.91	9.95	9.90	9.95	9.87	9.91	9.91	9.85	9.95
Al_{IV}	1.11	0.96	1.09	0.99	1.09	1.08	1.08	0.88	1.08	1.07	0.98	1.07
Al_{VI}	1.19	1.19	1.21	1.17	1.20	1.27	1.20	1.16	1.25	1.20	1.28	1.17
$T^\circ \pm 1\sigma$	295 ± 11	247	289 ± 12	257 ± 34	289 ± 7	286	284 ± 22	222 ± 11	284 ± 14	283 ± 16	254	283 ± 10

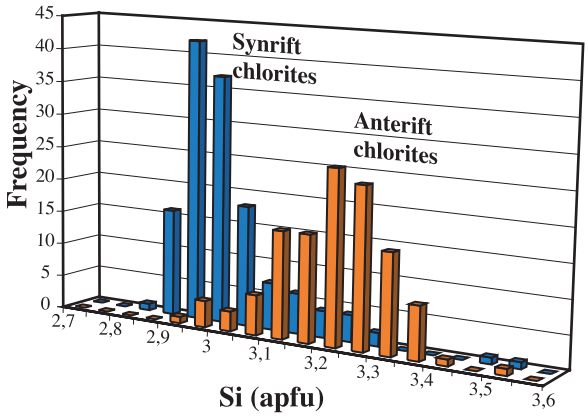

Figure 3. Frequency of Si-content in chlorites from ODP leg 180 core samples, expressed as the number of Si atoms per function unit (apfu). Red symbols, anterift chlorites; blue symbols, synrift chlorites.

with a peak frequency at 3.25 apfu. On the other hand, Si-content in synrift chlorites is in the range 2.85–3.35 apfu, with a sharp peak at 2.95 apfu. Synrift chlorites are therefore depleted in silica compared with anterift chlorites.

[14] Temperature estimates calculated from chlorite compositions are shown in Figure 4, and averaged in Table 1. At talus sites (1118 and 1109), temperature estimates lie between 190 and 240°C, with a peak frequency at 210°C (Figures 4c and 4d). No variation is observed between shallow and deeper core sections, or between anterift and synrift chlorites. On the other hand, the two generations of chlorites from footwall sites (1114 and 1117) yield striking temperature differences. Anterift chlorites yield a 180–250°C temperature range and a maximum frequency at 230°C similar to those of talus sites (1118 and 1109), whereas synrift chlorites yield temperatures in the range 270–320°C with a peak frequency at 290°C (Figures 4a and 4b). The temperature of crystallization of synrift chlorites was therefore 80 to 100°C higher than that of anterift chlorites. Note that the scatter of synrift chlorite temperatures is in the range 200–320°C at the bottom of the drilling holes, but only 270–320°C in the highest core sections beneath the faults. The closer to the fault scarps, the narrower the temperature range.

5.2. Fluid Inclusion Data

[15] Fluid inclusions were found in one sample of the secondary fault (site 1114) and four samples from the footwall of the main detachment (site 1117). Microthermometric results are shown in Figures 5 and 6. In sample 37Rcc29-32 (hole 1114A, 346 mbsf), ~10 μm large fluid inclusions occur in a zoned zeolite-quartz-chlorite vein in cataclasite. Zeolite grew on the vein walls. Quartz subsequently precipitated on the zeolite. Chlorite occupies the center of the vein. Primary fluid inclusions are found as isolated clusters in quartz not linked to any plane or trail. Secondary inclusions occur as trails in quartz, occasionally radiating from chlorite grains. This suggests that chlorite and secondary fluid inclusions are cogenetic. At low temperature, the first phase change observed during heating is the last melting of ice between −15 and −0.5°C. Salinity estimates are therefore regarded as bulk solution concentrations because no eutectic temperature is available. Salinity of primary fluid inclusions clusters between 10 and 15 wt% NaCl equivalent, while secondary inclusions show a sharp peak at 6 wt% NaCl equivalent (Figure 5a). No clathrate is found in either of the two inclusion types. Both primary and secondary inclusions homogenize to the liquid phase at 120–230°C (Figure 5a). Calculated densities fall in the range 0.98–1.02 $g.cm^{-3}$ for primary inclusions and a 0.90–0.95 $g.cm^{-3}$ for secondary inclusions. Consequently, density isochores of primary inclusions lie above those of secondary inclusions in the pressure-temperature (P-T) field (Figure 6a).

[16] In sample 14R1W1-3 (bottom of hole 1117A, 110 mbsf), 5–10 μm fluid inclusions are found in a quartz vein as trails parallel to the vein walls, and were likely trapped during the growth of the vein. In the heating stage, the first phase transition observed is the last melting of ice at −18 to −1.9°C. Corresponding salinities range from 4 to 22 wt% NaCl equivalent with no significant peak

Figure 4. Temperature of hydrothermal alteration deduced from chlorite compositions using the *Cathelineau and Nieva* [1985] geothermometer, as a function of the depth in the core sections in meters below sea level (mbsf). Red symbols and boxes correspond to anterift chlorites crystallized in static replacement of the primary magmatic mineralogy. Blue symbols and boxes correspond to synrift chlorites crystallizing in deformation microstructures. Each box is drawn by eye as the mean area of temperature values. The brown areas mark the overlap of red and blue boxes. Frequency stacks of temperatures are also reported below the temperature profiles (when the two sets of temperatures overlap, the lowest frequency is represented in foreground for clarity).

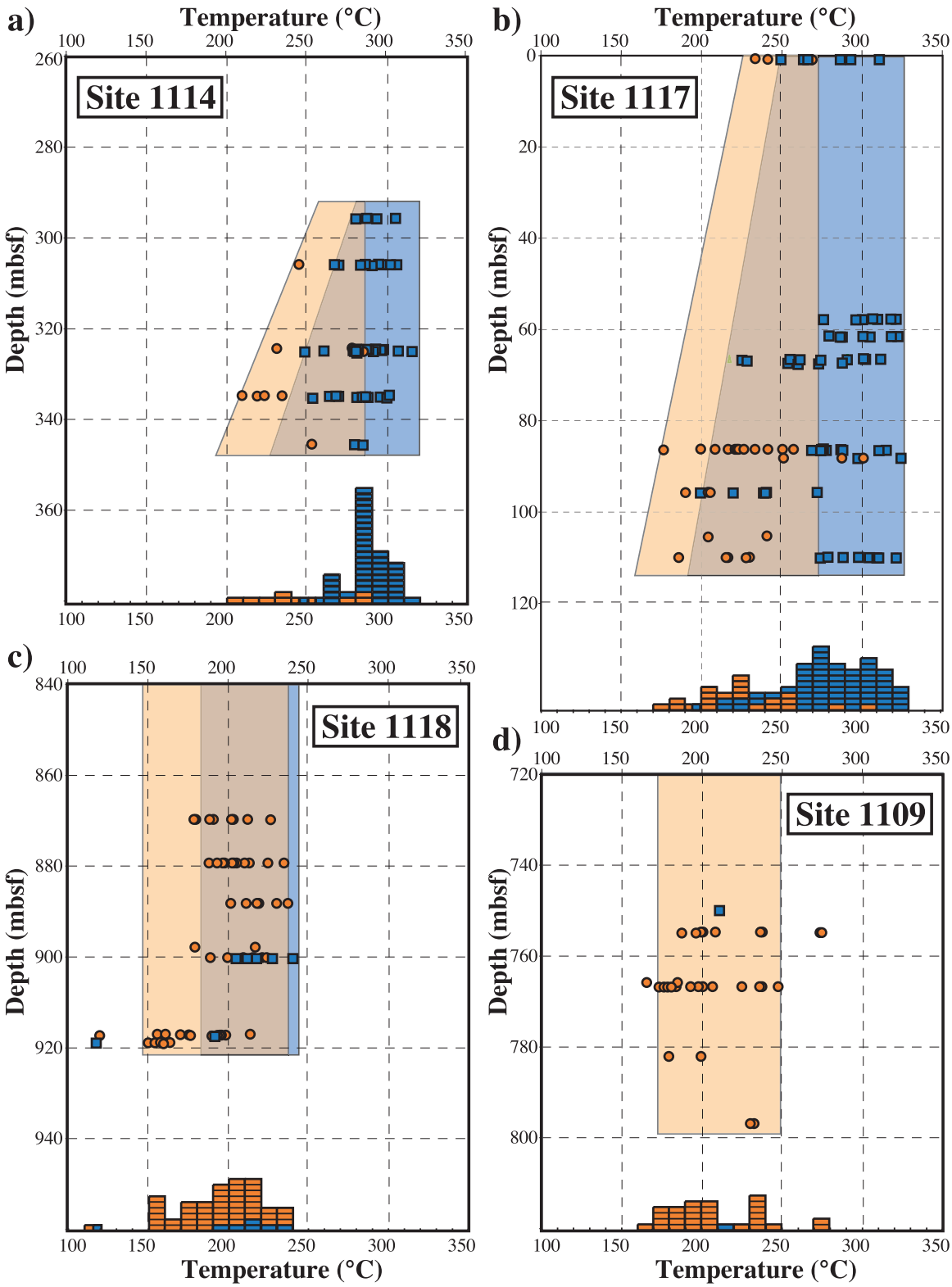
a)
Temperature (°C)
Site 1114
Depth (mbsf)
b)
Temperature (°C)
Site 1117
Depth (mbsf)
c)
Site 1118
Depth (mbsf)
Temperature (°C)
d)
Site 1109
Depth (mbsf)
Temperature (°C)

Figure 4

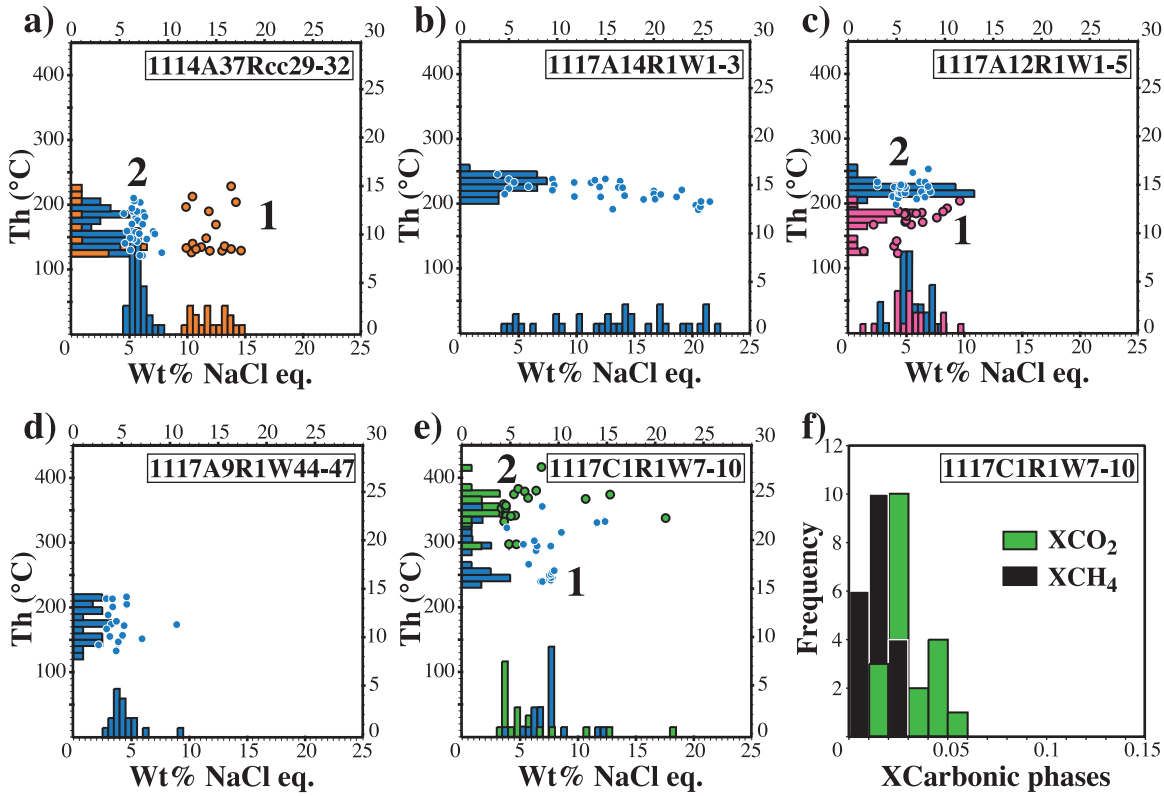

Figure 5. Microthermometric data on fluid inclusions. (a) Sample 37Rcc29-32 (345 mbsf, hole 1114A). (b–d) Samples 14R1W1-3 (110 mbsf), 12R1W1-5 (88 mbsf), and 9R1W44-47 (67 mbsf), respectively (hole 1117A). (e) Sample 1R1W7-10 (0.1 mbsf, hole 1117C). Three types of data are represented in these diagrams: Salinity frequency diagrams on the X axis (wt% NaCl equivalent), temperature of homogenization frequency diagrams on the Y axis (T_h), and salinity versus temperature of homogenization on XY plots. (f) Molar concentrations of CO_2 and CH_4 in carbon bearing fluid inclusions from sample 1R1W7-10. The colors and numbers appended to the data refer to chronological criteria detailed in text. When two sets of fluid inclusion data overlap, the lowest frequency is shown in foreground for clarity.

(Figure 5b). No clathrate is either found in these inclusions. Homogenization to liquid occurs between 200 and 260°C, with a peak at 220°C (Figure 5b). Density estimates lie between 0.92 and 1.01 g.cm^{-3}, yielding an unimodal repartition of isochores (Figure 6b).

[17] Fluid inclusions from sample 12R1W1-5 (hole 1117A, 88 mbsf) come from epidote-quartz-calcite and chlorite veins in fractured gabbro. Epidote grows on the vein walls. Quartz and calcite precipitate cogenetically and fill the veins after epidote. Chlorite occurs in microcracks crosscutting the epidote-quartz-calcite veins at high angle. Fluid inclusions occur in epidote, quartz and calcite as secondary planes oriented along two main directions: (1) Planes parallel to the vein walls that display small inclusions (≤5 μm) with a high degree of fill (≥90%). (2) Planes parallel to or radiating from chlorite microcracks, that crosscut and therefore postdate the first direction of planes. Inclusions in this second set are bigger (>5 μm) and show a lower degree of fill (≤80%). Upon heating, the first phase transition in all the inclusions occurs at −28 to −26°C, interpreted as the last melting of metastable hydrohalite in a pure H_2O-NaCl system. Last melting of ice occurs between −6.2 and −1.4°C, corresponding to a peak salinity at 5 wt% NaCl equivalent (Figure 5c). The next phase change is complete homogenization to liquid between 120 and 260°C, with a peak at 180°C for the first set and 230°C for the second set (Figure 5c). Density estimates are in the range 0.90–0.95 g.cm^{-3} for the first set and 0.84–0.87 g.cm^{-3} for the second set, yielding a bimodal distribution of isochores (Figure 6c).

[18] Fluid inclusions from sample 9R1W44-47 (hole 1117A, 67 mbsf) come from a quartz vein deformed by ductile creep within a mylonite matrix. Only a few tiny secondary fluid inclusions (~3 μm) were found in this sample. The first

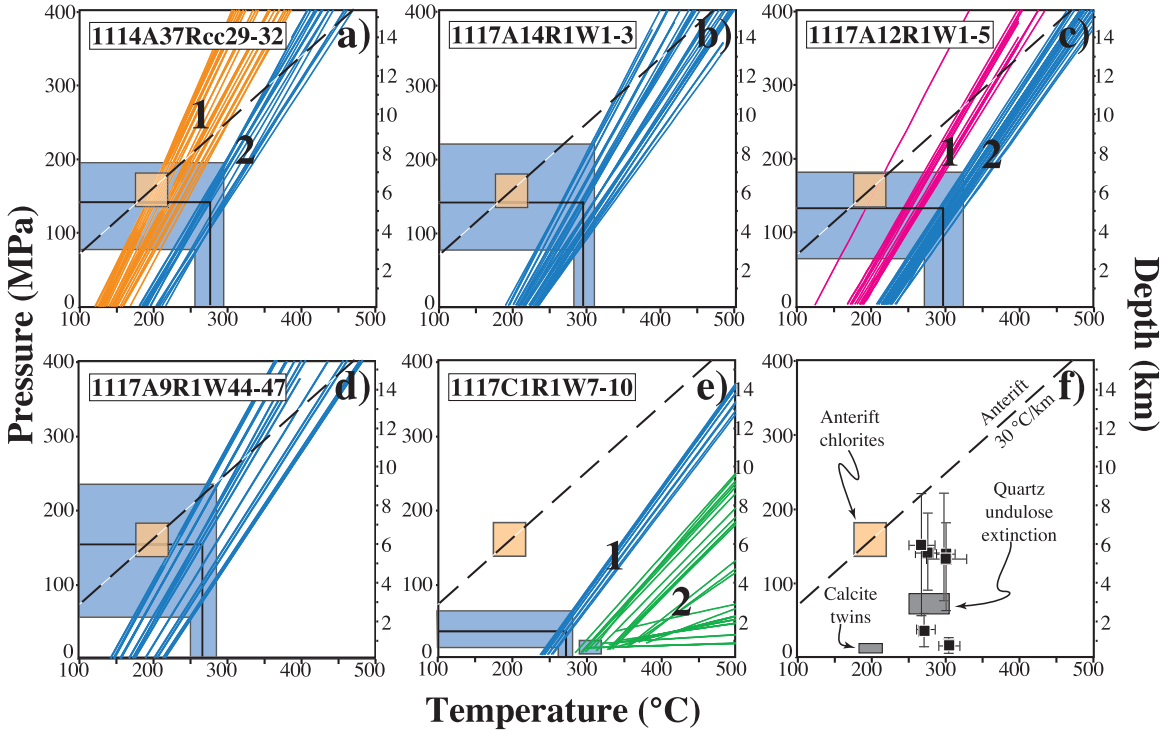

Figure 6. Calculated density isochores of fluid inclusions (see Figure 5 for microthermometric data). Blue areas represent the possible range of fluid pressures inferred from the projection of synrift chlorite temperatures on the isochores (see Table 1). The colors and numbers appended to the isochores refer to chronological criteria detailed in text. The red squared areas represent the P-T estimate for anterift greenschist retrogression [*Gardien et al.*, 2002]. The dashed lines represent the 30°C/km anterift geothermal gradient (assuming a rock density = 2.7 g·cm^{-3}). (a) Sample 37Rcc29-32 (346 mbsf, hole 1114A). (b–d) Samples 14R1W1-3 (110 mbsf), 12R1W1-5 (88 mbsf), and 9R1W44-47 (67 mbsf), respectively (hole 1117A). (e) Sample 1R1W7-10 (0.1 mbsf, hole 1117C). (f) Summary of pressure and temperature estimates. The gray squares represents the P-T estimates deduced from quartz ductility in mylonites and calcite twinning in late veins (both from *Roller et al.* [2001]).

observed phase transition is the last melting of ice at −5.7 to −1.7°C, yielding a peak salinity at 4 wt% NaCl equivalent (Figure 5d). Complete homogenization to liquid occurs between 120 and 220°C with no well-defined peak (Figure 5d). Density estimates of 0.87–0.96 g.cm^{-3} yield scattered isochores in the P-T field (Figure 6d), possibly because of a leakage of the inclusions during quartz deformation.

[19] Fluid inclusions from sample 1R1W7-10 (fault scarp in hole 1117C, 0.1 mbsf) were found in undeformed quartz-chlorite veins cutting across a mylonite matrix. Quartz and chlorite precipitated cogenetically. Two types of inclusions occur in this sample: (1) primary clouds of ~5 μm large inclusions cogenetic to the infill of the veins, and (2) secondary planes of 5–20 μm large inclusions cutting across the veins. Primary fluid inclusions show a high degree of fill (>80%). In these inclusions, the first phase transition at −28 to −23°C indicates the metastable last melting of hydrohalite. Last melting of ice occurs between −8 and −4°C, yielding a peak salinity at 7.5 wt% NaCl equivalent (Figure 5e). No clathrate is found in these inclusions. Complete homogenization to liquid occurs between 230 and 350°C, with a peak at 250°C (Figure 5e). Density estimates lie in the range 0.85–0.90 g.cm^{-3}, and isochores are therefore similar to those of the four other samples (Figure 6e). On the other hand, secondary fluid inclusions show a wide range of degree of fill from 0 to 90% at room temperature, even within a single inclusion plane. No evidence for necking down being observed, this indicates that two immiscible fluids, one liquid phase and one gas phase, were trapped at the same time at varying ratios. At low temperature, the first phase transition observed is the sublimation of carbonic compounds between −56.6 and −58°C, indicating that the inclusions contain a low-density CO_2-CH_4 mixture. The concentration of carbonic phases clusters between 0

and 5 mol% (Figure 5f). Ice melting is not observed due to the presence of carbonic phases, yet clathrate melting at 2.6 to 8.2°C indicates NaCl concentrations scattered from 3.5 to 17 wt% NaCl equivalent (Figure 5e). This scatter is typical of the "salting in" effect of CO_2 immiscibility on aqueous solutions [*Robert et al.*, 1995]. Homogenization occurs from 300°C to 400°C with no well-defined peak (Figure 5e). Homogenization mode is to the gas phase for fluid inclusions with a low liquid content, and to the liquid phase for inclusions with a high degree of fill. As pointed out by *Roedder* [1984], the homogenization temperatures of fluid inclusions trapped as a single fluid phase (liquid water or carbonic gas), i.e., the lowest temperature of homogenization values, give an estimate of the P-T of trapping. The lowest value obtained is ~300°C. Calculated densities range from 0.78 g.cm^{-3} for inclusions trapped as one liquid phase to 0.10 g.cm^{-3} for inclusions trapped as one gas phase. Corresponding density isochores crosscut at 10 to 50 MPa (Figure 6e).

6. Discussion

6.1. Temperature of Hydrothermal Alteration

[20] The Si content of anterift chlorites indicates that pre-detachment temperatures are in the range 180–220°C for all drilling sites (Figure 4). These results are in good agreement with previous estimates [*Gardien et al.*, 2002]. As suggested by the Si content of synrift chlorites, this thermal regime did not change in the hanging wall margin of the Moresby detachment during rifting (sites 1118 and 1109; Figures 4c and 4d). In contrast, synrift chlorites from 1114 and 1117 drilling sites show that a 280–320°C thermal overprint occurred in the footwall during rifting (Figures 4a and 4b). This +100°C increase over the anterift geotherm is also confirmed by the ductile deformation of quartz in mylonites [*Roller et al.*, 2001] and by the ~300°C trapping temperature of immiscible fluid inclusions in veins (Figures 5e and 6e). These data are in conflict with the cooling that should have occurred with the exhumation of footwall rocks along the low-angle normal fault. Importantly, the thermal overprint is restricted to the two fault zones in the footwall margin of the Moresby detachment, and therefore cannot be explained by an increase in the regional temperature gradient as a consequence of crustal rifting and thinning. Tectonic reconstructions, petrological data and stratigraphic correlations show that basement rocks did not experience any significant burial before or during the rifting stage that could either account for the temperature rise [*Huchon et al.*, 2002]. The temperature rise is also too steady over each drilling site, and over two sites distant of 2 km, to be either explained by shear heating alone. A more likely interpretation is that the +100°C overprint results from the circulation of hot hydrothermal fluids along the two fault zones. Fluids must have penetrated the fault zones at 300°C or more in order to account for the thermal event observed. The injection of hot fluids into the fault zone offers an explanation to the ductile deformation of quartz and the overprint of brittle deformation textures by mylonites observed in the cored sections. It is also worth noting that our temperature data are in striking agreement with the present-day heat anomaly up to 100°C/km measured at the surface of the Moresby detachment (Figure 2a), also interpreted as a circulation of hot fluids [*Shipboard Scientific Party*, 1999a]. The hydrothermal activity responsible for the synrift thermal overprint through the fault zones is probably still occurring nowadays.

6.2. Pressure Evolution of the Fluids

[21] Since fluid inclusions are found in association with synrift chlorites in most of the studied samples, the projection of chlorite temperatures on the density isochores of inclusions can be used to estimate the pressure of trapping. However, pressure estimates are not very precise due to the scatter of isochores, possibly because of fluid pressure fluctuations during trapping, as reported in other shear zones [*Parry and Bruhn*, 1986; *Robert et al.*, 1995]. In the following, we will nevertheless assume that pore pressure remained close to lithostatic during most of the activity of the two faults, an assumption which is supported by deformation microstructures, vein orientations and permeability measurements [*Kopf*, 2001; *Roller et al.*, 2001].

[22] In sample 37Rcc29-32 (hole 1114A), the isochores of primary fluid inclusions crosscut the 30°C/km anterift geotherm at a minimum of 200°C and 160 MPa (Figure 6a), in agreement with the conditions of anterift alteration. This suggests that the vein opened before the thermal event. In addition, the projection of the mean temperature from synrift chlorites (274 ± 17°C, Table 1) on the isochores of secondary inclusions yields a pressure of 140 ± 50 MPa (Figure 6a). Therefore the synrift temperature increase was nearly isobaric during vein development in sample 37Rcc29-32. In sample 14R1W1-3 (hole 1117A),

no chlorite was found in association with fluid inclusions in the quartz vein. However, the projection of the temperature from synrift chlorites in adjacent sample 14R1W 13–15 (299 ± 16°C, Table 1) yields a pressure of 140 ± 60 MPa (Figure 6b), as in sample 37Rcc29-32. The P-T conditions of rifting were therefore likely equal at the bottom of holes 1114A and 1117A. In sample 12R1W1-5 (hole 1117A), synrift chlorites (311 ± 18°C, Table 1) and the isochores of the second set of fluid inclusions yield a pressure estimate of 120 ± 40 MPa (Figure 6c). In sample 9R1W44-47 (hole 1117A), no synrift chlorites were found, but those from adjacent sample 9R1W80-83 yield a temperature of 266 ± 19°C (Table 1), or a rough pressure estimate of 160 ± 90 MPa by projection on fluid inclusion isochores (Figure 6d). In sample 1R1W7-10 (hole 1117C), synrift chlorites (266 ± 14°C, Table 1) and the isochores of H_2O-NaCl fluid inclusions gives a pressure estimate of 40 ± 20 MPa, well below that of other samples. This low pressure is confirmed by the crosscutting of carbonic fluid inclusions isochores at ~300°C and 10–50 MPa (Figure 6e). Therefore the sample collected at the fault scarp, likely the most lately reworked by deformation, recorded the latest P-T conditions, whereas the bottom of the cores preserved deeper and earlier conditions, as also suggested by the wedge shape of temperature profiles at footwall sites (1114 and 1117; Figures 4a and 4b).

[23] The P-T path of footwall rocks inferred from chlorite and fluid inclusions data is summarized in Figure 6f. The data depict a history of exhumation beginning with an isobaric temperature increase from 200 to 300°C, and followed by an isothermal decompression at 300°C from 150 MPa and 5–7 km to the subsurface. The fact that the thermal overprint began as an isobaric event implies that the circulation of hot fluids initiated before most of the vertical movement of the footwall. Hydrothermal fluids were therefore likely present from the very beginning of detachment formation, at the onset of rifting. The occurrence of high temperature chlorites even in the deepest, oldest and best preserved parts of the cored sections confirms this interpretation. Since then, hydrothermal circulation maintained this +100°C overheating during the whole exhumation of the footwall along the detachment, down to subsurface conditions.

6.3. Composition and Source of the Fluids

[24] According to the infill of veins at footwall sites, the composition of hydrothermal fluids evolved from a silica-rich solution in the deeper part of the drilling cores, to a calcite-and CO_2-rich solution beneath the faults scarps [*Shipboard Scientific Party*, 1999b]. Independently, microthermometric analyses of fluid inclusions indicate that fluid composition evolves from a medium salinity H_2O-NaCl solution (10–15 wt% NaCl equation, Figures 5a and 5b) at the beginning of deformation, to a low-salinity, carbon bearing solution (3–5 wt% NaCl equation; 0–5 mol% CO_2+CH_4, Figures 5a–5d) during the latest stage of shearing. The salinity of early fluids, higher than that of superficial fluids, is typical of a metamorphic source [*Schuiling et al.*, 1987; *Miller et al.*, 2002]. The low $\delta^{18}O$ and boron content of calcite veins also suggest that the hydrothermal fluids were produced by dehydration and decarbonation of high-grade metamorphic rocks [*Kopf et al.*, 2003]. Conversely, the $\delta^{13}C$ of late calcite veins and the analysis of C-O-H compounds in cores suggest that the late carbon fraction of the fluids is of biogenic origin [*Shipboard Scientific Party*, 1999a; *Kopf et al.*, 2003]. Mixing of metamorphic fluids with those surface-derived fluids could explain the low salinity of the most recent fluid inclusions trapped at shallow depth.

[25] At the onset of rifting, the source of fluids needs to have rooted at a minimum depth of 8 km in order to explain the ~300°C temperature (Figure 6f), assuming an anterift geotherm of 30°C/km as suggested by leg ODP 180 data [*Shipboard Scientific Party*, 1999a]. An alternative possibility, however, is that crustal thinning was already increasing the synrift geotherm toward the present-day value (~100°C/km) when the detachment fault formed. This would have allowed fluids to be heated at ~300°C from a shallower depth. In any case, the fact that most of the fluid inclusions were trapped at about 150 MPa implies that the source of fluids lies at a minimum depth of 5–7 km.

[26] In the continental part of the Woodlark Basin, the lower ductile crust is composed of metamorphic gneisses that breach over the Papuan ophiolites as the D'Entrecasteaux core complexes [*Martinez et al.*, 2001]. Accordingly, we therefore suggest that fluids are expelled from the metamorphic lower crust by dehydration and decarbonation, and move upward along the detachment fault from a minimum depth of 5–7 km. Those metamorphic fluids would have mixed with meteoric and biogenic fluids near the surface.

[27] These conclusions are somewhat contrasting with some previous studies, including of our own,

on detachments from the Basin and Range and the Aegean sea, showing a deep infiltration of surface-derived fluids down to the ductile shear zone [*Fricke et al.*, 1992; *Wickham and Peters*, 1992; *Wickham et al.*, 1993; *Famin and Nakashima*, 2004; *Famin et al.*, 2004]. The compilation of worldwide data suggests that detachment faults are systematically associated with a strong hydrothermal alteration of the fault zones, but that the source of fluids may vary from a detachment to another.

6.4. Mechanism of Fluid Release and Detachment Faulting

[28] The depth of the Mw = 6.2 earthquake that occurred along the Moresby detachment at 5.3 ± 0.2 km [*Abers et al.*, 1997] is strikingly similar to the depth of brittle veining and brecciation inferred from fluid inclusions data on the exhumed footwall. We therefore suggest that the similarity might not be fortuitous, and that a genetic link does exist between low angle earthquakes and the upward expulsion of deep-seated fluids (Figure 7). Earthquakes and faults require a low apparent coefficient of friction in order to initiate and slip at low angle. At the base of the brittle crust, this condition is reached if the pore pressure is equal or higher than the lithostatic load [*Axen*, 1992; *Rice*, 1992], or if metamorphic reactions involving fluids transform the hard minerals into weaker phyllosilicates [*Wintsch et al.*, 1995]. Results show that those fluids were supplied at 5–7 km below the seafloor since the beginning of faulting, and that they are probably still available nowadays. In addition, the temperature increase from 200°C to 300°C induced by the circulation of fluids may also participate to the weakening of rocks, not only by increasing the pore pressure and the rate of hydrothermal reactions, but also by activating ductile creep in minerals. By any of these weakening mechanisms, the upward flow of hot hydrothermal fluids is expected to create a weak point at the tip of the detachment fault. This weak point could be the locus of low angle earthquakes nucleation (Figure 7). Rupture cycles would in turn enhance the upward migration of fluids toward the surface.

[29] In a former paper, we have shown that a downward inflow of surface-derived fluids could explain the propagation of low angle detachment faults in the continental crust [*Famin et al.*, 2004]. Here, we suggest that the release of deep-seated fluids by dehydration and decarbonation of metamorphic rocks may also create a weak point in the middle crust. This weak point could trigger the localization of deformation into a low angle detachment fault, and the evolution of continental extension into an asymmetric rift bordered by core complexes.

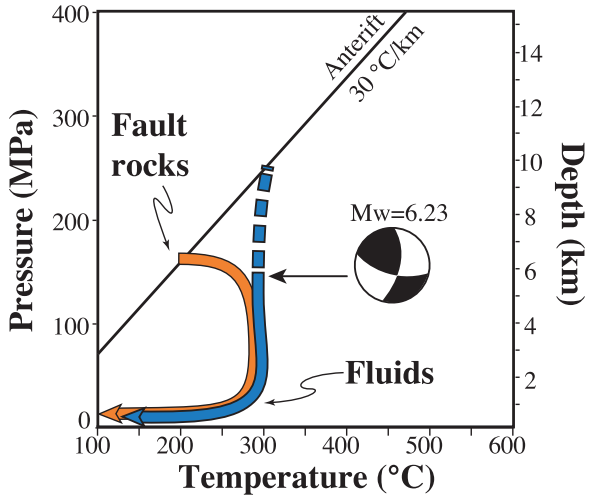

Figure 7. Sketch of pressure and temperature evolution in the footwall of the Moresby detachment fault. Red arrow: path of rocks from the fault zones undergoing exhumation. Blue arrow: path of fluids moving upward along the fault.

7. Conclusion

[30] In the Moresby rift, samples recovered from the leg ODP 180 campaign on an active, normal detachment show a strong hydrothermal alteration associated with synrift faulting. Chemical analyses of the thermodependent Si-Al substitutions in chlorites show that synrift alteration is coeval with a temperature rise from 200 to 300°C in the exhumed footwall of the fault, whereas no thermal event is recorded in the hanging wall. In the same samples, fluid inclusions show that footwall rocks followed an isothermal exhumation path from 5–7 km to the subsurface. Taken together, the results lead to the following conclusions: (1) The +100°C heating results from the upward migration of H_2O-NaCl fluids expelled by dehydration of metamorphic rocks from a depth of 5–7 km. (2) Fluid release began at the onset of detachment faulting, and is still actively occurring in the present. (3) The ~5 km depth at which deformation and hydrothermal alteration occurred in the exhumed footwall is also the depth of present-day low angle earthquakes occurring along the detachment fault. This reinforces the idea of a genetic link between

hydrothermal alteration and the development of low angle detachment faults in continental rifts.

Acknowledgments

[31] The authors wish to thank V. Gardien for providing the ODP samples. P. Huchon is acknowledged for insightful remarks on the Papuan geodynamics. T. Parra guided our use of chlorite geothermometers. S. Takeuchi is also thanked for his help during the EPMA analyses. The clarity of the manuscript benefited from the careful reviews by A. M. Boullier and A. Kopf. This research was funded by JSPS grants A212304034 to S. Nakashima and P1503798 to V. Famin.

References

Abers, G. A. (1991), Possible seismogenic shallow-dipping normal faults in the Woodlark-D'Entrecasteaux extensional province, Papua New Guinea, *Geology*, *19*, 1205–1210.

Abers, G. A., C. Z. Mutter, and J. Fang (1997), Earthquakes and normal faults in the Woodlark-d'Entrecasteaux rift system, Papua New Guinea, *J. Geophys. Res.*, *102*, 15,301–15,317.

Axen, G. (1992), Pore pressure, stress increase, and fault weakening in low-angle normal faulting, *J. Geophys. Res.*, *97*(B6), 8979–8991.

Baldwin, S. L., G. S. Lister, E. J. Hill, D. A. Foster, and I. McDougall (1993), Thermochronologic constraints on the tectonic evolution of active metamorphic core complexes, d'Entrecasteaux islands, Papua New Guinea, *Tectonics*, *12*(3), 611–628.

Bowers, T. S., and H. C. Helgeson (1983), Calculation of the thermodynamic and geochemical consequences of nonideal mixing in the system H_2O-CO_2-NaCl on phase relation in geologic systems: Equation of state for H_2O-CO_2-NaCl fluids at high pressures and temperatures, *Geochim. Cosmochim. Acta*, *47*, 1247–1275.

Brown, P. E. (1989), FLINCOR: A microcomputer program for the reduction and investigation of fluid inclusion data, *Am. Mineral.*, *74*, 1390–1393.

Cathelineau, M., and D. Nieva (1985), A chlorite solid solution geothemometer: The Los Azufres (Mexico) geothermal system, *Contrib. Mineral. Petrol.*, *91*, 235–244.

Davies, H. L., and R. G. Warren (1988), Origin of eclogite-bearing, domed, layered metamorphic complexes ("core complexes") in the D'Entrecasteaux islands, Papua New Guinea, *Tectonics*, *7*(1), 1–21.

Famin, V., and S. Nakashima (2004), Fluid migration in fault zones and the evolution of detachments: The example of Tinos Island (Greece), in *Physicochemistry of Water in Geological and Biological Systems—Structures and Properties of Thin Aqueous Films*, edited by S. Nakashima et al., pp. 189–209, Universal Acad., Tokyo.

Famin, V., P. Philippot, L. Jolivet, and P. Agard (2004), Evolution of hydrothermal regime along a crustal shear zone, Tinos Island, Greece, *Tectonics*, *23*, TC5004, doi:10.1029/2003TC001509.

Floyd, J. S., J. C. Mutter, A. M. Goodliffe, and B. Taylor (2001), Evidence for fault weakness and fluid flow within an active low-angle normal fault, *Nature*, *411*, 779–783.

Fricke, H. C., S. M. Wickham, and J. R. O'Neil (1992), Oxygen and hydrogen isotope evidence for meteoric water infiltration during mylonitization and uplift in the Ruby Mountains-East Humboldt Range core complex, Nevada, *Contrib. Mineral. Petrol.*, *111*, 203–221.

Gardien, V., B. LeGall, B. Celerier, V. Louvel, and P. Huchon (2002), Low pressure-temperature evolution of the continental crust exhumed during the opening of the Woodlark basin, in *Proc. Ocean Drill. Program*, *Sci. Results* [CD-ROM], *180*, 28 pp.

Glazner, A. F., and J. M. Bartley (1991), Volume loss, fluid flow and state of strain in extensional mylonites from the central Mojave Desert, California, *J. Struct. Geol.*, *13*(5), 587–594.

Hill, E. J., S. L. Baldwin, and G. S. Lister (1992), Unroofing of active metamorphic core complexes in the D'Entrecasteaux islands, Papua New Guinea, *Geology*, *20*, 907–910.

Huchon, P., B. Taylor, and A. Klaus (Eds.) (2002), *Proceedings of Ocean Drilling Program, Scientific Results*, vol. 180, Ocean Drill. Program, College Station, Tex.

Jolivet, L., V. Famin, C. Mehl, T. Parra, C. Aubourg, R. Hébert, and P. Philippot (2004), Strain localization during crustal-scale boudinage to form extensional metamorphic domes in the Aegean Sea, in *Gneiss Domes in Orogeny*, edited by D. L. Whitney, C. Teyssier, and C. S. Siddoway, *Spec. Pap. Geol. Soc. Am.*, *380*, 185–210.

Karner, G. D., N. W. Driscoll, and J. K. Weissel (1993), Response of the lithosphere to in-plane force variations, *Earth Planet. Sci. Lett.*, *114*(4), 397–416.

Kemerer, A., and E. Screaton (2002), Permeabilities of sediments from Woodlark basin: Implications for pore pressures, *Proc. Ocean Drill. Program, Sci. Results* [CD-ROM], *180*, 28 pp.

Kerrick, D. M., and G. K. Jacobs (1981), APL and FORTRAN programs for a new equation of state of H_2O, CO_2 and their mixture at supercritical conditions, *Comput. Geosci.*, *7*, 131–143.

Kopf, A. (2001), Permeability variation across an active low-angle detachment fault, western Woodlark Basin (ODP Leg 180), and its implication for fault activation, in *The Nature and Tectonic Significance of Fault Zone Weakening*, edited by R. E. Holdsworth et al., *Geol. Soc. Spec. Publ.*, *186*, 23–41.

Kopf, A., J. H. Behrmann, A. Deyhle, S. Roller, and H. Erlenkeuser (2003), Isotopic evidence (B, C, O) of deep fluid processes in fault rocks from the active Woodlark Basin detachment zone, *Earth Planet. Sci. Lett.*, *208*, 51–68.

Losh, S. (1997), Stable isotope and modeling studies of fluid-rock interaction associated with the Snake Range and Mormon Peak detachment faults, Nevada, *Geol. Soc. Am. Bull.*, *109*(3), 300–323.

Martinez, F., A. M. Goodliffe, and B. Taylor (2001), Metamorphic core complex formation by density inversion and lower crust extrusion, *Nature*, *411*, 930–934.

Miller, J. A., I. S. Buick, I. Cartwright, and A. Barnicoat (2002), Fluid processes during the exhumation of high-P metamorphic belts, *Mineral. Mag.*, *66*(1), 93–119.

Monteleone, B. D., S. L. Baldwinn, T. R. Ireland, and P. G. Fitzgerald (2002), Thermochronologic constraints for the tectonic evolution of the Moresby seamount, Woodlark Basin, Papua New Guinea, *Proceedings of Ocean Drill. Program*, *Sci. Results* [CD-ROM], *180*, 35 pp.

Morrison, J. (1994), Meteoric water-rock interaction in the lower plate of the Whipple Mountain metamorphic core complex, California, *J. Metamorph. Geol.*, *12*, 827–840.

Parry, W. T., and R. L. Bruhn (1986), Pore fluid and seismogenic characteristics of fault rock at depth on the Wasatch fault, Utah, *J. Geophys. Res.*, *91*(B1), 730–744.

Rice, J. (1992), Fault stress states, pore pressure distributions, and the weakness of San Andreas fault, in *Fault Stress States, Pore Pressure Distributions, and Transport Properties of Rocks: A Festschrift in Honor of W. F. Brace*, edited by B. Evans and T. F. Wong, pp. 475–503, Elsevier, New York.

Robert, F., A.-M. Boullier, and K. Firdaous (1995), Gold-quarts veins in metamorphic terranes and their bearing on the role of fluids in faulting, *J. Geophys. Res.*, *100*(B7), 12,861–12,879.

Roedder, E. (1984), *Fluid Inclusions*, *Rev. Mineral.*, vol. 12, 644 pp., Mineral. Soc. of Am., Washington, D. C.

Roller, S., J. H. Behrmann, and A. Kopf (2001), Deformation fabrics of faulted rocks, and some syntectonic stress estimates from the active Woodlark Basin detachment zone, in *Non-Volcanic Rifting of Continental Margins: A Comparison of Evidence From Land and Sea*, edited by R. C. L. Wilson et al., *Geol. Soc. Spec. Publ.*, *187*, 319–334.

Schmidt, C., and R. J. Bodnar (2000), Synthetic fluid inclusions: XVI. PVTX properties in the system H_2O-NaCl-CO_2 at elevated temperatures, pressures, and salinities, *Geochim. Cosmochim. Acta*, *64*(22), 3853–3869.

Schuiling, R. D., R. Kreulen, and J. Salemck (1987), Metamorphic events in the Cyclades and their associated fluids, in *Chemical Transport in Metasomatic Processes*, edited by H. C. Helgeson, pp. 451–466, Springer, New York.

Shipboard Scientific Party (1999a), *Proceedings of the Ocean Drilling Program, Initial Reports* [CD-ROM], edited by B. Taylor, P. Huchon, and A. Klaus, Ocean Drill. Program, College Station, Tex.

Shipboard Scientific Party (1999b), Site 1117, *Proc. Ocean Drill. Program, Init. Rep.* [CD-ROM], *180*, 134 pp.

Sibson, R. H. (1985), A note on fault reactivation, *J. Struct. Geol.*, *7*, 751–754.

Taylor, B., and P. Huchon (2002), Active continental extension in the Woodlark Basin: A synthesis of leg 180 results, *Proc. Ocean Drill. Program, Sci. Results*, *180*, 36 pp.

Weissel, J. K., and A. B. Watts (1979), Tectonic evolution of the Coral Sea Basin, *J. Geophys. Res.*, *84*, 4572–4582.

Wernicke, B. P. (1981), Low-angle normal faults in the Basin and Range province: Nappe tectonics in an extending orogen, *Nature*, *291*, 645–648.

White, S. H., and R. J. Knipe (1978), Transformation- and reaction-enhanced ductility in rocks, *J. Geol. Soc. London*, *135*, 513–516.

Wickham, S. M., and M. T. Peters (1992), Oxygen and carbon isotope profiles in metasediments from Lizzies Basin, East Humbolt Range, Nevada: Constraints on mid-crustal metamorphic and magmatic volatile fluxes, *Contrib. Mineral. Petrol.*, *112*, 46–65.

Wickham, S. M., M. T. Peters, H. Fricke, and J. R. O'Neil (1993), Identification of magmatic and meteoric fluid sources and upward- and downward-moving infiltration fronts in a metamorphic core complex, *Geology*, *21*, 81–84.

Wintsch, R. P., R. Christoffersen, and A. K. Kronenberg (1995), Fluid-rock reaction weakening of fault zones, *J. Geophys. Res.*, *100*(B7), 13,021–13,032.

Zoback, M. D., et al. (1985), New evidence on the state of stress of the San Andreas fault system, *Science*, *238*, 1105–1111.